Discovery and pharmacological characterization of JNJ-42756493 (erdafitinib), a functionally selective small molecule FGFR family inhibitor

Timothy P.S. Perera[1], Eleonora Jovcheva[1], Laurence Mevellec[2], Jorge Vialard[1], Desiree De Lange[1], Tinne Verhulst[1], Caroline Paulussen[1], Kelly Van De Ven[1], Peter King[1], Eddy Freyne[1], David C. Rees[3], Matthew Squires[3], Gordon Saxty[3], Martin Page[1], Christopher W. Murray[3], Ron Gilissen[1], George Ward[3], Neil T. Thompson[3], David R. Newell[4], Na Cheng[5], Liang Xie[5], Jennifer Yang[5], Suso J. Platero[6], Jayaprakash D. Karkera[6], Christopher Moy[6], Patrick Angibaud[2], Sylvie Laquerre[6] and Matthew V. Lorenzi[6,7].

[1]Janssen Research and Development, Beerse, Belgium.

[2]Janssen Research and Development, Val de Reuil, France.

[3]Astex Pharmaceuticals, Cambridge, United Kingdom.

[4]Newcastle Cancer Centre, Northern Institute for Cancer Research, Newcastle University, Newcastle upon Tyne, UK.

[5]Janssen Research and Development, Shanghai, China.

[6]Janssen Research and Development, Spring House, USA.

[7]To whom correspondence should be addressed: Matthew V. Lorenzi, Oncology Discovery, Janssen R&D, 1400 McKean Road, Spring House, PA 19477. Phone: 215 793-7356; E-mail: mlorenzi@its.jnj.com

Disclosure of Potential Conflicts of Interest: T.P.S. Perera, E. Jovcheva, L. Mevellec, J. Vialard, D. De Lange, T. Verhulst, C. Paulussen, K. Van De Ven, P. King, E. Freyne, M. Page, R. Gilissen, N. Cheng, L. Xie, J. Yang, S.J. Platero, J.D. Karkera, C. Moy, P. Angibaud, S. Laquerre and M.V. Lorenzi are or have been employees of Janssen R&D, and D.C. Rees, M. Squires, G. Saxty, C.W. Murray, G. Ward and N.T. Thompson, are or have been employees of Astex Pharmaceuticals. The authors disclose no additional financial support.

Manuscript information: Abstract: 160 words, total: 5560 words, 5 figures and 1 table. Supplementary Material: 1 figure, 4 tables.

Running title: Preclinical characterization of erdafitinib
Keywords: FGFR inhibitor, lung cancer, lysosomal, structure-based design
Specific Categories: Small Molecule Therapeutics

Abstract

Fibroblast growth factor (FGF) signaling plays critical roles in key biological processes ranging from embryogenesis to wound healing and has strong links to several hallmarks of cancer. Genetic alterations in FGF receptor (FGFR) family members are associated with increased tumor growth, metastasis, angiogenesis and decreased survival. JNJ-42756493, erdafitinib, is an orally active small molecule with potent tyrosine kinase inhibitory activity against all four FGFR family members and selectivity versus other highly related kinases. JNJ-42756493 shows rapid uptake into the lysosomal compartment of cells in culture, which is associated with prolonged inhibition of FGFR signaling, possibly due to sustained release of the inhibitor. In xenografts from human tumor cell lines or patient-derived tumor tissue with activating FGFR alterations, JNJ-42756493 administration results in potent and dose-dependent antitumor activity accompanied by pharmacodynamic modulation of phospho-FGFR and phospho-ERK in tumors. The results of the current study provide a strong rationale for the clinical investigation of JNJ-42756493 in patients with tumors harboring FGFR pathway alterations.

Introduction

Fibroblast growth factor receptors belong to a family of 4 receptor tyrosine kinases (FGFR1-4) and a 5th receptor (FGFR5) lacking a tyrosine kinase domain (1, 2). FGFRs have been demonstrated to regulate a number of key processes such as cell migration, proliferation, differentiation and survival, particularly during embryonic development and in the adult organism during inflammation and wound healing (1, 2). FGFR activity is controlled by a

family of FGF ligands, comprised of 22 FGF members (3) that regulate FGFR tyrosine kinase activity in an autocrine or paracrine tissue-dependent context (4). A key example of FGFR ligand-regulated physiology is the regulation of phosphate homeostasis mediated by FGF23 which suppresses phosphate reabsorption in proximal tubules of the kidney (5). In contrast, constitutive ligand-independent and aberrant ligand-dependent FGFR signaling have been described in a large variety of solid tumors including non-small cell lung, breast, bladder, endometrial, gastric and colon cancer, as well as certain hematological malignancies. Aberrant pathway activation is believed to be a key growth promoting mechanism for these malignancies (1-16). Further support of this concept is highlighted by the presence of activating FGFR gene alterations, including point mutations and gene rearrangements, in multiple tumor types, suggesting that deregulated proliferation of certain tumors is driven by these oncogenic events (7, 17). Given the activation of FGFR signaling in a variety of tumor types, several therapeutic agents, including multiple FGFR inhibitors, FGFR antibodies and FGF ligand traps, have been optimized and have been tested clinically or are entering into clinical development (18). Most of these small molecule inhibitors have limited selectivity for FGFR and display significant activity against additional protein tyrosine kinases due to high sequence homology within their kinase domains (e.g. vascular endothelial growth factor [VEGFR], platelet-derived growth factor [PDGFR] and c-Kit). The activities of these mixed FGFR/VEGFR inhibitors makes it difficult to dissect the anti-tumor activity components associated with FGFR inhibition versus other inhibitory events leading to potential additional toxicities compared to selective inhibitors.

To better address the role of constitutive FGFR signaling in cancer, we optimized a next generation small molecule inhibitor that is highly selective for the FGFR kinase family with minimal inhibitory activity towards VEGFR and other related kinases. Here we report the identification and pharmacological characterization of JNJ-42756493 (erdafitinib) as a novel,

highly potent and selective, small-molecule inhibitor of FGFR1-4. This study demonstrates functional selectivity of erdafitinib in tumor models with constitutive FGFR activity and supports the ongoing clinical development of this agent in disorders associated with FGFR activation.

Materials and Methods

JNJ-42756493

JNJ-42756493 (Fig. 1A), N-(3,5-Dimethoxy-phenyl)-N'-isopropyl-N-[3-(1-methyl-1 *H*-pyrazol-4-yl)-quinoxalin-6-yl]-ethane-1,2-diamine, was synthesized according to the processes described in the International Patent Application Number WO2011/135376 in particular as described for example B3 (compound 4). JNJ-42756493 (446.56MW of free base) has no chiral center, is basic (pKa of 9.2) and lipophilic (logP=4.3). It is a crystalline, auto-fluorescent (Exc 370nm; Emm 490nm), non-hygroscopic solid, with a melting point of 142°C and a high thermodynamic solubility of >20mg/mL in aqueous buffer at pH=4. JNJ-42756493 in 5mM dimethyl sulphoxide (DMSO) stock was used for *in vitro* or was formulated for *in vivo* studies in 20% hydroxypropyl-β-cyclodextrin (HP-β-CD) for oral gavage either once or twice daily.

Time-resolved fluorescence kinase assays for FGFR1-4 and KDR

Time-resolved fluorescence energy-transfer assays for FGFR1-4 and KDR were performed in 384-well black Optiplates (Perkin Elmer, 6007279). Enzymes (FGFR1 (Upstate, 14-582-4)

FGFR2 (Invitrogen, PV4106), FGFR3 (Upstate, 14-464-K), FGFR4 (Upstate, 14-593-K) and KDR (Upstate, 14-630-K)), substrate (FLT 3 peptide, Bachem, 4072151) and adenosine triphosphate (ATP, Invitrogen, PV3227) were prepared in 50mM HEPES pH 7.5, 0.1mM Na_2VO_3, 6 $MnCl_2$, 0.01% (v/v) Triton x-100 and 1mM dithiothreitol (DTT). Detection reagents were prepared in 6.25mM HEPES, 0.025% BSA, 7mM EDTA, 31.25nM streptavidin-XL665

(CISBIO, 610SAXLB) and 2.27nM Eu-labeled PY20 antibody (Perkin Elmer, AD0067). The kinase reaction was initiated by addition of enzyme (0.1, 0.8, 0.8, 0.4 and 0.7nM of FGFR 1, 2, 3, 4 and KDR, respectively) to a mixture containing compound, ATP at the Michaelis constant (Km) concentration for each kinase (5, 0.4, 25, 5, and 3µM, respectively) and 500nM FLT3 substrate in a final assay volume of 30µL. After 60min for FGFR1, FGFR3 and KDR, 30min for FGFR2 and 45min for FGFR4 incubation at room temperature, the enzyme reaction was stopped by adding 10µL of detection reagents. Following 1hr incubation at room temperature, fluorescence was measured with excitation at 337nm and dual emission at 620nm (Eu signal) and 665nm (FRET signal) on an Envision reader (Perkin Elmer, 2104-0010A).

Kinase binding assays

The binding affinity of JNJ-42756493 to a panel of 397 wild type kinases was evaluated using the KINOMEscan platform (DiscoveRx) (19).

Cellular kinase assays

Interleukin-3 (IL-3)-dependent (10ng/ml final concentration) murine BaF3 (Riken Cell Bank) pro-B cells (20) were transfected with pcDNA3.1 (Invitrogen) plasmid encoding TEL(ETV6)-kinase and stable integrations selected with geneticin (Invitrogen) (21). GFP-TEL-FGFR1 and GFP-TEL-KDR(VEGFR2) were kindly provided by Jan Cools (Department of Human Genetics, University of Leuven).

Cell lines

The tumor cell lines used for western blotting and the small panel tested in proliferation experiments were obtained from the American Type Culture Collection (ATCC, Manassas, VA,

USA), unless specified otherwise. KATO III (HTB-103), SNU-16 (CRL-5974), RT-112 (DSMZ ACC 418), NCI-H1581 (CRL-5878), A-204 (HTB-82), RT-4 (HTB-2), DMS-114 (CRL-2066), A-427 (HTB-53), KMS-11 (Japanese Collection of Research Bioresources), and MDA-MB-453 (HTB-131) cells were selected to reflect diverse FGFR alterations. All cell lines were obtained between 2012-2016 and kept in culture up to 15-20 passages, but not longer than 6 months. All cell lines were authenticated by the suppliers using short tandem repeat (STR) analysis. Cells were cultured as suggested by the supplier in standard culture conditions (37°C, 5% CO_2, 95% humidity) in medium containing10% (v/v) fetal bovine serum. Kato III cells were supplemented with 2mM L-glutamine, 1.5g/L sodium bicarbonate, 50µg/mL gentamycin and 20% fetal bovine serum. Cells were free of mycoplasma.

The cell lines tested in the extended panel of the growth assay were obtained from the American Type Culture Collection (22), the German Collection of Microorganisms and Cell Cultures (23), and the Japanese Collection of Research Bioresources (24) and cultured as described above.

Cell lines were annotated for somatic alterations using the data compiled by OmicSoft® ArraySuite® software, version 8. Original source data is derived from the Cell Line Encyclopedia (https://www.broadinstitute.org/ccle/home) and Sanger Center Cancer Cell Line Project, available on the COSMIC website (http://cancer.sanger.ac.uk/cosmic).

MTT assay for cell proliferation

KATO III, RT-112, A-204, RT-4, DMS-114, A-427 and MDA-MB-453 cells were treated with JNJ-42756493 (from 10µM to 0.01nM in 2% DMSO, final concentration). Following 4-day

incubation, cell viability was determined using MTT reagent as described by the supplier (Sigma, CGD1). The optical density was determined at 540 nm as a percentage of DMSO treated cells (100%), a dose response curve was created, and the median inhibition concentration (IC_{50}) calculated.

Alamar Blue assay for cell proliferation

SNU-16, NCI-H1581, KMS-11 and BaF3cells were treated with compound for 4 days as described above. Alamar Blue solution was added as described by the manufacturer (Sigma, R7017) and incubated for an additional 4hrs. Fluorescence was measured (excitation wavelength 530-560nm, emission wavelength 590nm) and expressed as a percentage of untreated control. From these data, a dose response curve was created and IC_{50} values determined.

Large panel all cancer and lung cancer cell lines.

Cancer cells were grown as specified by the provider (Oncolead, GmbH & Co. KG). At 24h post seeding, cells were treated in triplicate with small-molecule FGFR inhibitor serially diluted 3.16-fold over 10 concentrations (0.5% DMSO final concentration). Following 72h incubation, cells were fixed and stained with a nuclear dye for quantification of proliferation. To determine the cell proliferation endpoint, data were transformed to percent of control (POC) values (100X relative cell count [drug treatment]/relative cell count [vehicle treatment]). IC_{50} values were estimated from a nonlinear regression fit of the POC data to a 1-site dose-response model.

Inhibition of FGFR family receptor phosphorylation and downstream signaling

Cell lines harboring activated FGFR1, 2, 3, or 4 (NCI-H1581, SNU-16, KMS-11 and MDA-MB453, respectively) were treated with various concentrations of JNJ-42756493 for 4h. Medium was removed, cells washed with ice-cold phosphate buffered saline (PBS) and suspended in lysis buffer for western blotting analysis.

NCI-H1581 NSCLC cell line was pretreated with medium containing 100nM JNJ-42756493 or DMSO for 30 minutes prior to replacement with medium containing FGF2 (40ng/ml). The cells treated with FGF2 were incubated for 0min (control, no treatment with FGF2), 5min, 10min, 30min, 2hrs, 4hrs or 8hrs.The medium was aspirated, the cells were washed with ice-cold PBS, lysed and processed for western blot analysis.

Western blotting

Cell lysates were loaded on NuPAGE Novex Bis-Tris Mini Gels and transferred to poly vinylidene-difluoride (PVDF) membranes. Primary antibodies were incubated as specified, membrane washed 3 times in PBS-0.1% Tween-20, and fluorescently labeled secondary antibody incubated for 1hr at room temperature in the dark. Membranes were washed 3 times and antibody binding detected using Lumi Proxima or LiCOr Odyssey instruments. Antibodies against ERK, pERK (Thr202/Tyr204), pFGFR (Tyr653/654), pPLCg1(Tyr783) were obtained from Cell Signalling (#9101, #9102, #3471, # 2821, respectively), FGFR2 and FRS2α from Santa Cruz (SC #3471, SC #8318, respectively), and β-Actin from Calbiochem (# CP01). Secondary antibodies were obtained from Invitrogen (goat anti-rabbit IgG HRP (A21076), goat anti-mouse IgG HRP (A21057), goat anti-mouse (A21057), and goat anti-rabbit (A21076)).

Lysosomal compound accumulation

GAMG human glioblastoma cells, (DSMZ, ACC 242), were treated for 30 min with 50nM LysoTracker® red and 1μM JNJ-42756493 before imaging at 530nm. GAMG cells were treated with bafilomycin (75 nM) for 1h and washed with PBS before addition of medium supplemented with 1μM JNJ-42756493 or JNJ-42883919 in the presence or absence of 75nM bafilomycin. Serial images were obtained every 5 min (ImageJ) in Texas Red and CFP channels on an InCell Analyzer 2000 instrument. The density of region of interest (ROI) from 4 different images was compared to T=0 and the average difference plotted as percentage change (%ROI).

Drug washout assays

KATO III human gastric carcinoma cells were treated with or without bafilomycin (150nM) for 1h before addition of JNJ-42756493 (30nM) or JNJ-42883919 (300nM) to the culture medium. The medium was removed, cells were washed 6 times with warm medium with or without bafilomycin, and then incubated in medium lacking compounds and bafilomycin. Cells were collected at 0, 2, 4, 8, 16 and 24h, lysates prepared and processed for WES capillary-based western blotting as described by the manufacturer (ProteinSimple).

***In vivo* efficacy experiments**

All experiments were carried out in accordance with the European Communities Council Directives (86/609/EEC) and approved by the local IACUC and ethical committee. For tumor efficacy studies, tumor sizes (tumor Volume [mm^3] = [a x b^2/2]; where 'a' represents the length, and 'b' the width of the tumor as determined by caliper measurements) and body weights were measured twice weekly, with mice monitored daily for clinical signs of toxicity (including but not limited to persistent anorexia, dehydration, posture, lethargy [according to the United Kingdom Coordinating Committee for Cancer Research [UKCCCR] guidelines for welfare of

animals in experimental neoplasia]) (25) for the duration of the treatment. A sustained body weight loss >15% of the initial body weight was considered as clinical toxicity, with the animal removed from the study and sacrificed. Studies were terminated when tumor burden exceeded 10% of the animal's body weight. Time-course of tumor growth was expressed as relative tumor volumes, normalized to initial tumor volume (day treatment started) and expressed as mean±standard error of mean (SEM). Treatment/control (T/C) ratios were calculated based on the change in final relative tumor volumes, and National Cancer Institute's (NCI) effective criteria of 42% was used (26).

Human tumor cell lines were injected directly into the inguinal region of male nude mice ($1x10^7$ cells/200µL/animal with Matrigel® 1:1 in medium) on Day 0. When tumors were established, mice were randomized according to tumor volume to either vehicle alone (10% HP-β-CD) or vehicle containing JNJ-42756493, administered in a volume of 5mL/kg body weight for 21 days (8-10 mice/group). For PDX studies, Nu/Nu nude mice purchased from Vital River Lab Animal Technology Co., Ltd., Beijing, China. Patient-derived tumor samples finely minced (~1-2mm^3) were added to Matrigel and ~50mm^3 of minced tumor was implanted subcutaneously (s.c.) into flank of anaesthetized mice (Ketamine/Medatomidine). When the tumor volume reached 200-300mm^3 the mice were allocated to their treatment groups with uniform mean tumor volume and body weight between groups and treated according to protocol.

Pharmacodynamic and pharmacokinetic analysis of JNJ-42756493

Mice bearing SNU-16 human gastric carcinoma (FGFR2 amplified) xenograft tumors were dosed orally with 0, 3, 10 or 30mg/kg JNJ-42756493. Tumor tissue and mouse plasma (3 mice per time point) were harvested at 0.5, 1, 3, 7, 16 and 24h post-dosing. Tumor tissues were frozen in liquid nitrogen, crushed and suspended in lysis buffer (25mM Tris-HCl [pH 7.5], 2mM EDTA

[pH 8], 2mM EGTA [pH8], 1% Triton X-100, 0.1% SDS, 50mM disodium β-glycerophosphate, 2mM Na_3VO_4, 4mM Na-pyrophosphate, 2x Thermo protease/phosphatase inhibitor cocktail). After centrifugation (12,000rpm for 15 min; RCF=15,294), the supernatants were applied to SDS-PAGE and transferred onto PVDF membranes (BioRad, #162-0177). The membranes were blocked in Odyssey blocking buffer (Licor, #927-40000) for 1 hour, incubated with anti-phospho-FGFR Y653/654 (Cell Signaling Technology, #3471) or anti-FGFR2 (Cell Signaling Technology, #9102) antibodies overnight at 4°C, and washed 3 times in TBST buffer prior to incubation with Alexa Fluor 680 conjugated goat-anti-rabbit IgG (#A-21109) in Odyssey blocking buffer at room temperature for 2 hours. Signals were read and quantitated on a Licor Odyssey infrared imager.

When tumors of lung cancer patient-derived xenograft (PDX, LUX001) reached ~400mm^3, mice were dosed orally with 12.5mg/kg JNJ-42756493. Tumor and mouse plasma (3 mice per time point) were collected at 1, 2, 4, 8, and 24h post dose. The liquid nitrogen frozen tumor tissues were lysed in RIPA buffer containing protease inhibitor (Roche, Cat#04693132001) and phosphatase inhibitor (Roche, Cat#04906837001). After centrifugation (12,000rpm for 15 min), the supernatants were applied to SDS-PAGE and transferred onto PVDF membranes (BioRad #170-4157). Membrane was blocked in 5% bovine serum albumin in Tris-buffered saline with 0.1% Tween 20 (TBST) and then incubated with anti-phospho-ERK (Cell Signaling Technology, #4370) overnight at 4°C, washed in TBST, then incubated with HRP-conjugated Goat Anti-Rabbit IgG (H+L) (BioRad, 1706515) at room temperature for 2 hours. The membranes were stripped and re-blotted for total ERK1/2 (Cell Signaling Technology, #9102). Signal was read on ChemiDocTM MP Imaging System.

Compound concentration from mouse plasma was detected using LC/MS/MS.

Results

JNJ-42756493 is a potent and selective pan-FGFR inhibitor

The hinge binding motif, quinoxaline scaffold of JNJ-42756493 (**Table 1**), was identified following a fragment based screen of the Astex proprietary library (20). Quinoxaline containing fragments were further modified by introducing the 3,5-dimethoxy aniline moiety beyond the gatekeeper in the selectivity pocket. Taking advantage of aniline nitrogen positioning, substituents interacting with Asp641 were introduced that ultimately led to selection of JNJ-42756493, a potent inhibitor of FGFR1, FGFR2, FGFR3 and FGFR4 (FGFR1-4) kinases (**Table 1**).

JNJ-42756493 inhibited the tyrosine kinase activities of FGFR1-4 in time-resolved fluorescence assays with IC_{50} values of 1.2, 2.5, 3.0 and 5.7nM, respectively. The closely related VEGFR2 kinase was less potently inhibited (~30-fold less potent compared to FGFR1) by JNJ-42756493, with an IC_{50} value of 36.8nM.

The binding affinity of JNJ-42756493 was tested against a panel of 451 kinases (supplemental Table S1) using the KINOMEscan platform (DiscoveRx) (19). The 20 kinases with the highest binding affinity are shown in **Table 1**. JNJ-42756493 bound FGFR1, 3, 4, and 2 with Kd values of 0.24, 1.1, 1.4 and 2.2nM, respectively. The Kd value for VEGFR2 was somewhat higher at 6.6nM.

The potent kinase binding and inhibitory activities of JNJ-42756493 observed on the isolated recombinant FGFR kinases were recapitulated in BaF3 cell lines engineered to express FGFR family members. JNJ-42756493 inhibited proliferation of FGFR1, 3, and 4 expressing cells with IC_{50} values of 22.1, 13.2, and 25nM, respectively (**Table 1**). The specificity of JNJ-42756493 activity in these cells was confirmed by the absence of effects on proliferation in the presence of IL-3 (IC_{50} >7000nM for all cell lines tested). In contrast with the relatively potent activities against VEGFR2 in biochemical assays, JNJ-42756493 demonstrated substantially weaker activity against BaF3 cells expressing VEGFR2 (IC_{50} =1160nM) (**Table 1**). Similarly, JNJ-42756493 was at least 10-times more potent on BaF3 cells expressing FGFR kinases than other kinases with high binding affinities (RET, PDGFRA, PDGFRB, KIT, TIE1, LCK, LYN, ABL1 and BLK). To confirm that selectivity of JNJ-42756493 for FGFRs versus VEGFR was compound dependent and not assay related, Brivanib (BMS-540215), a dual VEGFR/FGFR inhibitor, was tested in the same biochemical and BaF3 cellular kinase assays. In contrast to JNJ-42756493, Brivanib demonstrated higher potency against VEGFR2 compared to FGFRs (**Supplemental Table S2**), consistent with previous reports (27). Collectively, these results highlight the biochemical and functional selectivity of JNJ-42756493 for the FGFR family with limited off-target activity against VEGFR2 and other kinases.

Cellular activity of JNJ-42756493 and inhibition of downstream signaling

As demonstrated in **Fig. 1A**, JNJ-42756493 effectively inhibited pFGFR1, pFGFR3 and pFGFR4 at 100nM in NCI-H1581, KMS-11 and MDA-MB-453 cells, respectively, and pFGFR2 at 30nM in SNU-16 cells. Inhibition of FGFR auto-phosphorylation was consistent with its anti-proliferative IC50s in these cell lines (2.6, 0.40, 102.4, and 129.2 nM, for NCI-H1581, SNU-16, KMS-11 and MDA-MB-453, respectively) (**Table 1**). The inhibitory activity of JNJ-42756493

on proliferation was confirmed in several additional cell lines with FGFR alterations from multiple cancer types (**Table 1**).

The inhibitory activity of JNJ-42756493 on signal transduction pathways downstream of FGFR was assessed in NCI-H1581, a lung cancer cell line with a focal *FGFR1* gene amplification (**Fig. 1B**). To activate downstream signaling, cells were stimulated with FGF2 ligand. In DMSO pre-treated samples, robust FGFR pathway activation was detected within 5min of ligand addition, as evidenced by higher levels of pFGFR and pFRS2 (FGFR adaptor protein), as well as increased phosphorylation of Phospholipase C gamma 1 (pPLCγ1) and Extracellular Signal Receptor Regulated Kinase 1 and 2 (pERK1/2). Pretreatment with JNJ-42756493 for 1hr prior to addition of FGF2 ligand, led to inhibition of downstream signaling, evidenced by decreased levels of pFGFR, pFRS2, pPLCγ1 and pERK1/2. Taken together these data demonstrate cellular pan-FGFR kinase inhibition by JNJ-42756493 leading to modulation of FGFR downstream signaling.

Potent anti-proliferative activity of JNJ-42756493 on FGFR altered cancer cell lines

The anti-proliferative selectivity of a close analogue of JNJ-42756493, JNJ-42541707 (**Supplemental Fig. S1A**), was tested against large panel of human cancer cell lines of diverse tissue origin. Sensitivity (IC_{50} <1μM) was observed in a subset of the tumor cell lines and largely correlated with overexpression of FGFR family members (**Supplemental Fig. S1B**). A similar analysis using a slightly different panel of cancer cell lines was performed with JNJ-42756493. Interestingly, in addition to a correlation of sensitivity with FGFR overexpression, a large fraction of insensitive tumor cell lines harbored mutations in RAS or RAF indicating that

alterations downstream of FGFR can overcome the effects of FGFR inhibition (**Fig. 2A** and underlying data on **Table S3**). The majority of cell lines tested were not sensitive to the inhibitor (IC_{50} > 5μM), highlighting its selectivity and confirming a lack of appreciable non-FGFR off-target activity.

To further understand the FGFR anti-proliferative relationship we extended testing to a broad panel of lung cancer cell lines. JNJ-42756493 activity in a panel of 145 lung cancer cell lines was associated with FGFR1 amplification status (**Fig. 2B**). However, not all lung cancer cell lines with FGFR1 amplification were sensitive to JNJ-42756493. Most of the insensitive tumor cell lines were found to co-harbor other known oncogenic mutations within the EGFR/KRAS pathway (**Fig. 2C**), indicating that these pathways may be more dominant oncogenic drivers in this context. The molecular determinants of cell lines sensitive to JNJ-42756493 between 1 and 5μM is unknown, but could be due to alternative FGFR activating mechanisms, such as chromosomal translocations, or FGFR-unrelated activities of JNJ-42756493. Taken together, our results highlight the functional selectivity of JNJ-42756493 for FGFR altered pathway without concomitant MAPK pathway alterations.

Intracellular lysosomal localization of JNJ-42756493 results in sustained pathway inhibition

Imaging of cells treated with JNJ-42756493, which is intrinsically fluorescent, revealed an intracellular staining pattern similar to that of the lysosomal marker LysoTracker®, consistent with lysosomal accumulation (**Fig. 3A**). Addition of bafilomycin, a specific inhibitor of the vacuolar-type H^+-ATPase that increases lysosomal pH, reduced lysosomal accumulation of LysoTracker® Red and JNJ-42756493 (**Fig. 3B**), but had little or no effect on the subcellular

distribution or accumulation of JNJ-42883919, another fluorescent FGFR inhibitor from the same chemical series as JNJ-42756493 (**Fig. 3C**). Time course analysis demonstrated rapid uptake and intracellular accumulation of JNJ-42756493 that was prevented by pre-treatment of the cells with bafilomycin (**Fig. 3E**).

Since JNJ-42756493 appears to accumulate to high concentrations in lysosomes, we speculated that this property of the compound might contribute to persistent FGFR kinase inhibition in cells. KATO III cells were treated with JNJ-42756493 or the non-lysosomotropic analogue, JNJ-42883919, for 1h, and FGFR2 inhibition (pFGFR) assessed following compound washout. The pFGFR signal was completely inhibited by JNJ-42756493 up to 4 hours, returning to basal levels 24 hours after washout (**Fig. 3D**). In stark contrast, pFGFR levels in cells treated with JNJ-42883919 returned to basal levels within 2 hours. Pre-treatment of the cells with bafilomycin reversed sustained target inhibition by JNJ-42756493, as evidenced by detection of pFGFR at basal levels 2 hours after washout (**Fig. 3D**). Bafilomycin treatment did not alter the duration of pFGFR inhibition by the non-lysosomotropic analogue, JNJ-42883919. These data highlight the unique lysosomal accumulating properties of JNJ-42756493 that contribute to prolonged FGFR inhibition, possibly as a consequence of sustained release of the inhibitor over time.

JNJ-42756493 anti-tumor activity is associated with inhibition of FGFR downstream signaling.

We next assessed *in vivo* efficacy of JNJ-42756493 on tumors with FGFR alterations. Animals bearing xenograft tumors derived from SNU-16 human gastric cancer cells harboring FGFR2 amplifications were treated orally with vehicle or JNJ-42756493 at various doses. Upon administration, JNJ-42756493 reached maximal plasma concentration at 0.5h and returned to undetectable levels (lower limit of quantification (LLOQ) = 0.4ng/ml) by 7h for the 3 mg/kg dose, and 16h for the 10 and 30 mg/kg doses. No significant inhibition of downstream FGFR

signaling was observed in tumor lysates from mice treated with 3mg/kg JNJ-42756493 (**Fig. 4A**). However, FGFR signaling was significantly inhibited, starting from 1h after administration until 7h and 16h, in mice treated with 10 (**Fig. 4B**) and 30mg/kg (**Fig. 4C**) of JNJ-42756493, respectively. Significant inhibitor-dependent modulation of pERK was not consistently observed in this tumor model. The reasons are unknown, but could be due to technical reasons, such as the presence of mouse stromal cells with reactivity to the pERK antibody. Nevertheless, JNJ-42756493 resulted in dose-dependent tumor growth inhibition (TGI) in SNU-16 tumor-bearing mice. Treatment with 10 and 30 mg/kg JNJ-42756493 daily for 21 days resulted in TGI of 37.8% and 59.4%, respectively (**Fig. 4D**). Similar anti-tumoral effects were observed in several other tumor models (MDA-MB-453, SNU-16, NCI-H1581, A-204, HuH-7, NCI-H716 and RT112) with a variety of different FGFR alterations (**Supplemental Table S4.**).

In addition to gene amplification or overexpression, FGFRs can be constitutively activated by chromosomal rearrangement (7, 28). However, FGFR gene translocations are rarely present in existing xenograft models derived from cancer cell lines. To examine the dependency of tumors with FGFR translocations to JNJ-42756493, we surveyed a collection of patient-derived explant xenograft (PDX) models for FGFR genetic alterations and identified LUX001 (human non-small cell lung cancer (NSCLC)) that contains a translocation resulting in expression of a FGFR3-TACC3 fusion protein. LUX001-tumor (~400mm^3) bearing mice were treated with JNJ-42756493 for 21 days at 12.5 mg/kg twice a day (BID). Blood and tumors were collected before (t=0) and after first dosing with JNJ-42746493 for determination of concentration of the inhibitor in plasma and pERK inhibition in tumors (**Fig. 5A**). Similar to our observations in FGFR amplified models (**Fig. 4**), JNJ-42756493 treatment resulted in maximal plasma concentration at ~1hour post treatment, which was accompanied by suppression of constitutive pERK signaling

observed in this model. In this model, reduced plasma concentrations of the inhibitor were associated with decreased pERK suppression. Importantly, JNJ-42756493 resulted in pronounced anti-tumor activity (TGI=100%) in LUX001 tumor bearing mice treated suggesting that tumors harboring FGFR translocations are highly dependent upon this genetic activation event (**Fig. 5B**). These results demonstrated that the FGFR selective inhibitor JNJ-42756493 has potent *in vivo* activity on tumors with a variety of different FGFR genetic alterations.

Discussion

Targeted therapies against key activating genetic mutations have become standard of care for a variety of cancer subtypes. These developments have encouraged the field to mount new drug discovery efforts against emerging pathways such as FGFR, which has been observed to be activated at significant frequency in a variety of cancers (1). However, it is not clear if the observed mutations are bystander events or bona fide genetic drivers, particularly in tumor types such as lung cancer with high mutational burden. Further, confirmation of the oncogenic dependency on specific kinases using small molecule inhibitors that are not selective for the target of interest is complicated by off-target activities that can inhibit other anti-proliferative pathways and/or can be associated with toxicities limiting therapeutic utility. Thus, highly selective inhibitors such as JNJ-42756493 can be useful tools for determining the dependency of tumors on oncogenic driver pathways such as FGFR and may reduce the risk of off-target adverse events. Clinical data obtained with JNJ-42756493 so far is consistent with the hypothesis supporting absence of appreciable VEGFR2 inhibitory activity (29).

Our data highlight the functional selectivity of JNJ-42756493 for the FGFR family in a variety of model systems. First, unlike first-generation mixed FGFR/VEGFR inhibitors such as Brivanib, which are more potent against VEGFR than FGFR (30), JNJ-42756493 demonstrated greater than 50-fold selectivity over VEGFR2 in cellular assays. Second, broad *in vitro* anti-proliferative profiling of tumor cell lines with JNJ-42756493 revealed that sensitivity was associated with FGFR overexpression or amplification, whereas insensitivity was associated with the activation of other oncogenic pathways. Interestingly, the majority of tumor cell lines with FGFR aberrations that were resistant to JNJ-42756493 harbored additional mutations in RAS or RAF family members, indicating that mutations downstream of the receptor tyrosine kinase can bypass dependency on the receptor. These observations are consistent with what has been

reported for EGFR and downstream KRAS mutations (31, 32) and have clinical implications for the use of anti-EGFR agents such as cetuximab, which are not indicated in colorectal cancer patients with KRAS alterations (33). Our data have similar clinical implications suggesting that patient co-harboring FGFR mutations and downstream RAS or RAF mutations are not likely to be sensitive to pathway inhibition by JNJ-42756493.

A consequence of FGFR activation is the phosphorylation of downstream signal transducers such as FRS2 and ERK2 (34). We observed a strong correlation between levels of JNJ-42756493 and the suppression of FGFR auto-phosphorylation and downstream signaling events *in vitro*. Similarly, we observed sustained inhibition of pFGFR and pERK following administration of JNJ-42756493 in xenograft and PDX models, respectively. The reasons for the absence of pERK modulation in the xenograft model described are unclear, but pERK modulation in a patient-derived xenograft with an activating FGFR3-TACC3 translocation resulted in a robust anti-tumor activity. Similarly, patients harboring FGFR2 or FGFR3 translocations have also shown response to JNJ-42756493 treatment (29). It is not clear whether anti-tumor efficacy is driven by maximum concentration (Cmax), total area under the curve (AUC) or prolonged trough concentration (Ctrough) levels. The transient decrease in pERK after JNJ-42756493 administration suggests that sustained exposure over a threshold rather that Cmax exposure is more closely associated with efficacy. In this regard, it is interesting to note that JNJ-42756493 accumulates in lysosomes, which can potentially serve as a depot for sustained release of the compound and result in more prolonged pathway inhibition.

There is increasing interest in targeting FGFR for cancer therapy due to its activation by point mutation, amplification or chromosomal rearrangement (1) in a variety of tumors. Activating FGFR gene rearrangements were first identified in a search for novel oncogenes in osteosarcoma. *FGFR2-FRAG1* was characterized as a potent oncogene consisting of FGFR2

with a C-terminal fusion of the FRAG1 dimerization sequence that promoted constitutive activation of the chimeric protein (35). This observation was recently extended clinically with the identification of multiple C-terminal fusion partners across most of the FGFR family members (36, 37) broadening the range of genetic alterations from known point mutations and gene amplification events. However, it is not clear if all these alterations confer equivalent dependency to tumor cells with a given FGFR alteration. *In vitro*, the impact of JNJ-42756493 on cell proliferation was evident in cancer cell lines of diverse tissue origin carrying amplifications in FGFR family members. Although the cell line panel tested in this study did not contain tumor cells with FGFR translocations we have since shown potent anti-proliferative effects in BaF3-FGFR3-TACC3 engineered cells (J.D. Karkera; personal communication), suggesting that this is also a dominant oncogenic event. However, *in vivo,* our results suggest that JNJ-42756493 is more potent in models with FGFR translocations compared to those with amplifications, implying that there is a hierarchy of dependency amongst the different FGFR genetic alterations. Nonetheless, these results support the clinical evaluation of JNJ-42756493 (29) in malignancies and other disorders associated with constitutively activated FGFR signaling.

References

1. Hallinan N, Finn S, Cuffe S, Rafee S, O'Byrne K, Gately K. Targeting the fibroblast growth factor receptor family in cancer. Cancer Treat Rev. 2016;46:51-62.
2. Wesche J, Haglund K, Haugsten EM. Fibroblast growth factors and their receptors in cancer. Biochem J. 2011;437:199-213.
3. Touat M, Ileana E, Postel-Vinay S, Andre F, Soria JC. Targeting FGFR Signaling in Cancer. Clin Cancer Res. 2015;21:2684-94.
4. Itoh N, Ornitz DM. Functional evolutionary history of the mouse Fgf gene family. Dev Dyn. 2008;237:18-27.
5. Dienstmann R, Rodon J, Prat A, Perez-Garcia J, Adamo B, Felip E, et al. Genomic aberrations in the FGFR pathway: opportunities for targeted therapies in solid tumors. Ann Oncol. 2014;25:552-63.
6. Lim SM, Kim HR, Shim HS, Soo RA, Cho BC. Role of FGF receptors as an emerging therapeutic target in lung squamous cell carcinoma. Future Oncol. 2013;9:377-86.
7. Wu YM, Su F, Kalyana-Sundaram S, Khazanov N, Ateeq B, Cao X, et al. Identification of targetable FGFR gene fusions in diverse cancers. Cancer Discov. 2013;3:636-47.
8. Schildhaus HU, Nogova L, Wolf J, Buettner R. FGFR1 amplifications in squamous cell carcinomas of the lung: diagnostic and therapeutic implications. Transl Lung Cancer Res. 2013;2:92-100.
9. Williams SV, Hurst CD, Knowles MA. Oncogenic FGFR3 gene fusions in bladder cancer. Hum Mol Genet. 2013;22:795-803.
10. Katoh M, Nakagama H. FGF receptors: cancer biology and therapeutics. Med Res Rev. 2014;34:280-300.
11. Penault-Llorca F, Bertucci F, Adelaide J, Parc P, Coulier F, Jacquemier J, et al. Expression of FGF and FGF receptor genes in human breast cancer. Int J Cancer. 1995;61:170-6.
12. Matsumoto K, Arao T, Hamaguchi T, Shimada Y, Kato K, Oda I, et al. FGFR2 gene amplification and clinicopathological features in gastric cancer. Br J Cancer. 2012;106:727-32.
13. Tsujimoto H, Sugihara H, Hagiwara A, Hattori T. Amplification of growth factor receptor genes and DNA ploidy pattern in the progression of gastric cancer. Virchows Arch. 1997;431:383-9.
14. Marian C, Ochs-Balcom HM, Nie J, Kallakury BV, Ambrosone CB, Trevisan M, et al. FGFR2 intronic SNPs and breast cancer risk: associations with tumor characteristics and interactions with exogenous exposures and other known breast cancer risk factors. Int J Cancer. 2011;129:702-12.
15. Spinola M, Leoni V, Pignatiello C, Conti B, Ravagnani F, Pastorino U, et al. Functional FGFR4 Gly388Arg polymorphism predicts prognosis in lung adenocarcinoma patients. J Clin Oncol. 2005;23:7307-11.
16. Dieci MV, Arnedos M, Andre F, Soria JC. Fibroblast growth factor receptor inhibitors as a cancer treatment: from a biologic rationale to medical perspectives. Cancer Discov. 2013;3:264-79.
17. Tanner Y, Grose RP. Dysregulated FGF signalling in neoplastic disorders. Semin Cell Dev Biol. 2016;53:126-35.
18. Katoh M. FGFR inhibitors: Effects on cancer cells, tumor microenvironment and whole-body homeostasis (Review). Int J Mol Med. 2016;38:3-15.
19. Fabian MA, Biggs WH, 3rd, Treiber DK, Atteridge CE, Azimioara MD, Benedetti MG, et al. A small molecule-kinase interaction map for clinical kinase inhibitors. Nat Biotechnol. 2005;23:329-36.
20. Daley GQ, Baltimore D. Transformation of an interleukin 3-dependent hematopoietic cell line by the chronic myelogenous leukemia-specific P210bcr/abl protein. Proc Natl Acad Sci U S A. 1988;85:9312-6.

21. Squires M, Ward G, Saxty G, Berdini V, Cleasby A, King P, et al. Potent, selective inhibitors of fibroblast growth factor receptor define fibroblast growth factor dependence in preclinical cancer models. Mol Cancer Ther. 2011;10:1542-52.
22. atcc.org [Internet]. American Type Culture Collection, USA; c2016 [cited 2016 Aug 26]. Available from: http://www.atcc.org/.
23. dsmz.de [Internet]. German Collection of Microorganisms and Cell Cultures, Germany; c1998-2015 [cited 2016 Aug 26]. Available from: http://www.dsmz.de/.
24. cellbank.nibiohn.go.jp [Internet]. Japanese Collection of Research Bioresources, Japan; c2005-2015 [cited 2016 Aug 26]. Available from: http://cellbank.nibiohn.go.jp/.
25. United Kingdom Co-ordinating Committee on Cancer Research (UKCCCR) Guidelines for the Welfare of Animals in Experimental Neoplasia (Second Edition). Br J Cancer. 1998;77:1-10.
26. Bissery MC, Chabot GG. [History and new development of screening and evaluation methods of anticancer drugs used in vivo and in vitro]. Bull Cancer. 1991;78:587-602.
27. Diaz-Padilla I, Siu LL. Brivanib alaninate for cancer. Expert opinion on investigational drugs. 2011;20:577-86.
28. Costa R, Carneiro BA, Taxter T, Tavora FA, Kalyan A, Pai SA, et al. FGFR3-TACC3 fusion in solid tumors: mini review. Oncotarget. 2016;7:55924-38.
29. Tabernero J, Bahleda R, Dienstmann R, Infante JR, Mita A, Italiano A, et al. Phase I Dose-Escalation Study of JNJ-42756493, an Oral Pan-Fibroblast Growth Factor Receptor Inhibitor, in Patients With Advanced Solid Tumors. J Clin Oncol. 2015;33:3401-8.
30. Cai ZW, Zhang Y, Borzilleri RM, Qian L, Barbosa S, Wei D, et al. Discovery of brivanib alaninate ((S)-((R)-1-(4-(4-fluoro-2-methyl-1H-indol-5-yloxy)-5-methylpyrrolo[2,1-f][1,2,4] triazin-6-yloxy)propan-2-yl)2-aminopropanoate), a novel prodrug of dual vascular endothelial growth factor receptor-2 and fibroblast growth factor receptor-1 kinase inhibitor (BMS-540215). J Med Chem. 2008;51:1976-80.
31. Young A, Lou D, McCormick F. Oncogenic and wild-type Ras play divergent roles in the regulation of mitogen-activated protein kinase signaling. Cancer Discov. 2013;3:112-23.
32. Benvenuti S, Sartore-Bianchi A, Di Nicolantonio F, Zanon C, Moroni M, Veronese S, et al. Oncogenic activation of the RAS/RAF signaling pathway impairs the response of metastatic colorectal cancers to anti-epidermal growth factor receptor antibody therapies. Cancer Res. 2007;67:2643-8.
33. Lievre A, Bachet JB, Boige V, Cayre A, Le Corre D, Buc E, et al. KRAS mutations as an independent prognostic factor in patients with advanced colorectal cancer treated with cetuximab. J Clin Oncol. 2008;26:374-9.
34. Kouhara H, Hadari YR, Spivak-Kroizman T, Schilling J, Bar-Sagi D, Lax I, et al. A lipid-anchored Grb2-binding protein that links FGF-receptor activation to the Ras/MAPK signaling pathway. Cell. 1997;89:693-702.
35. Lorenzi MV, Horii Y, Yamanaka R, Sakaguchi K, Miki T. FRAG1, a gene that potently activates fibroblast growth factor receptor by C-terminal fusion through chromosomal rearrangement. Proc Natl Acad Sci U S A. 1996;93:8956-61.
36. Gallo LH, Nelson KN, Meyer AN, Donoghue DJ. Functions of Fibroblast Growth Factor Receptors in cancer defined by novel translocations and mutations. Cytokine Growth Factor Rev. 2015;26:425-49.
37. Parker BC, Engels M, Annala M, Zhang W. Emergence of FGFR family gene fusions as therapeutic targets in a wide spectrum of solid tumours. J Pathol. 2014;232:4-15.

Figure Legends

Figure 1: JNJ-42756493 inhibits FGFR auto-phosphorylation in cancer cells lines with activated FGFR1-4 and FGFR dependent signaling in NCI-H1581 cells. **A)** Western blots of phospho-FGFR (pFGFR) and protein loading control actin in human cancer cell lines containing FGFR1-4 alterations following treatment with multiple JNJ-42756493 concentrations. **B)** Western blots of several phospho-proteins in FGFR signaling pathway and loading control proteins PLCγ1 and ERK1 in NCI-H1581 cells pre-treated with DMSO or JNJ-42756493, then stimulated for indicated length of time with FGF2.

Figure 2: JNJ-42756493 anti-proliferative activity against human cancer cell lines. JNJ-42756493 growth inhibition (IC_{50}) of cancer cell lines **A)** from multiple origin (n=236) and color coded based on RAS/RAF status, **B)** from lung cancer origin (n=136) and color coded based on FGFR1 focal DNA amplification. **C)** Subset of lung cancer cell lines with FGFR1 amplification color coded based on JNJ-42756493 sensitivity (green: IC_{50}<1000nM, red: IC_{50}>1000M) and with their corresponding RAS/EGFR status**.**

Figure 3: Lysosomal accumulation of JNJ-42756493 and sustained inhibition of FGFR following compound washout. GAMG cells showing **A)** intrinsic fluorescence of JNJ-427556493 (green), fluorescence of a lysosome staining probe (LysoTracker, red), and merging of the 2 images (Merged, yellow). **B)** Reduced lysosomal fluorescence intensity of JNJ-42756493 and LysoTracker in presence of bafilomycin **C)** absence of changes in JNJ-42883919 fluorescence intensity compared to LysoTracker in presence of bafilomycin. **D)** Sustained inhibition of pFGFR following washout of KATO III cells pre-treated with JNJ-42756493 compared to cells pre-treated with JNJ-42756493 and bafilomycin or pre-treated with JNJ-42883919 with and without bafilomycin. Western blot of actin as loading control. **E)** Florescence signal (530nm) in GAMG cells treated with JNJ-42756493 in the presence or absence of bafilomycin compared to T=0 in Region of Interest (% ROI).

Figure 4: Relationship between *in vivo* JNJ-42756493 plasma concentration, inhibition of pFGFR2 and efficacy in SNU-16 human gastric xenograft mouse model. Animals were treated with JNJ-42756493 at **A)** 3mg/kg, **B)** 10mg/kg or **C)** 30mg/kg QD. Tumor and blood from 3 animals per group were harvested after single first dose at indicated time points for analysis of pFGFR/FGFR2 by western blot ((left axis (gray bars), significant (P-value< 0.001) difference compared to T=0 is marked with asterisks) and plasma compound concentration (right axis, LLOQ=0.4mg/ml, black line), respectively. **D)** Efficacy of JNJ-42756493 was evaluated at 0 (vehicle), 3, 10 and 30mg/kg QD treatment for 21 days. Significant percent tumor growth inhibition (%TGI) of compound compared to vehicle treated animals is indicated at efficacious doses.

Figure 5: Relationship between *in vivo* JNJ-42756493 plasma concentration, inhibition of pERK and efficacy in LUX001 PDX with FGFR3-TACC3 fusion mouse model. Animals were treated with vehicle or JNJ-42756493 at 12.5mg/kg BID. **A)** At indicated time (0, 1, 2, 4, 8 and 24h) post-first dosing, blood and tumors from 3 animals per group were harvested for plasma compound concentration (right axis) and level pERK/Total-ERK by quantified western blot (left axis, significant (P-value<0.001) difference compared to T=0 is marked with asterisks), respectively. **B)** Efficacy of JNJ-42756493 was evaluated and percent tumor growth inhibition (%TGI) of compound compared to vehicle treated animals is indicated.

Author Manuscript Published OnlineFirst on March 24, 2017; DOI: 10.1158/1535-7163.MCT-16-0589
Author manuscripts have been peer reviewed and accepted for publication but have not yet been edited.

JNJ-42756493	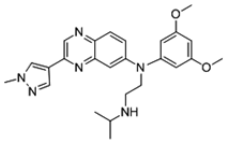			
Kinases	**Kd (nM)**	**Kinases**	**IC_{50} (nM)**	**+/- SD**
FGFR1	0.24	FGFR1	1.2	0.4
RET	0.94	FGFR2	2.5	0.9
FGFR3	1.1	FGFR3	3	0.5
FGFR4	1.4	FGFR4	5.7	0.8
FGFR2	2.2	VEGFR2	36.8	7.1
CSF1R	3.4	**Kinases**	**BaF3 IC50 (nM)**	**+/- SEM**
PDGFRA	3.4			
FLT4	3.6	FGFR1	22.1	0.81
PDGFRB	4.6	FGFR3	13.2	0.47
KIT	5.3	FGFR4	25	0.3
VEGFR2	6.6	VEGFR2	1160	30.7
TIE1	9	RET	205.2	25.7*
FLT1	12	PDGFRA	156.2	51.2*
EPHA1	13	PDGFRB	304.1	119.6*
LCK	20	KIT	>3000	N/A
LYN	22	TIE1	>3000	N/A
ABL1	23	LCK	>3000	N/A
EPHB6	32	LYN	646.4	197.5*
BLK	44	ABL1	>3000	N/A
DDR1	45	BLK	5514.2	567.6*
Cell line	**Origin**	**FGFR alteration**	**IC_{50} nM**	**+/- SEM**
KATO III	Gastric	FGFR2 (Amp)	0.1	0.01
SNU-16	Gastric	FGFR2 (Amp)	0.4	0.02
RT-112	Bladder	FGFR3 (translocation)	1.3	0.2
NCI-H1581	Large Cell Lung	FGFR1 (Amp)	2.6	0.2
A-204	Rhabdomyosarcoma	FGFR4 (Amp)	4.5	0.4
RT-4	Bladder	FGFR3 (translocation)	5.1	0.6
DMS-114	Small Cell Lung	FGFR1 (Amp)	7.0	1.2
A-427	Squamous Lung	FGFR1 (Amp)	71.0	25.6
KMS-11	Multiple Myeloma	FGFR3 (translocation)	102.4	53.6
MDA-MB-453	Breast	FGFR4 (Y367C)	129.2	30.4

*+/- SD

Table 1: Biochemical and cellular inhibitory activity of JNJ-42756493

Figure 1

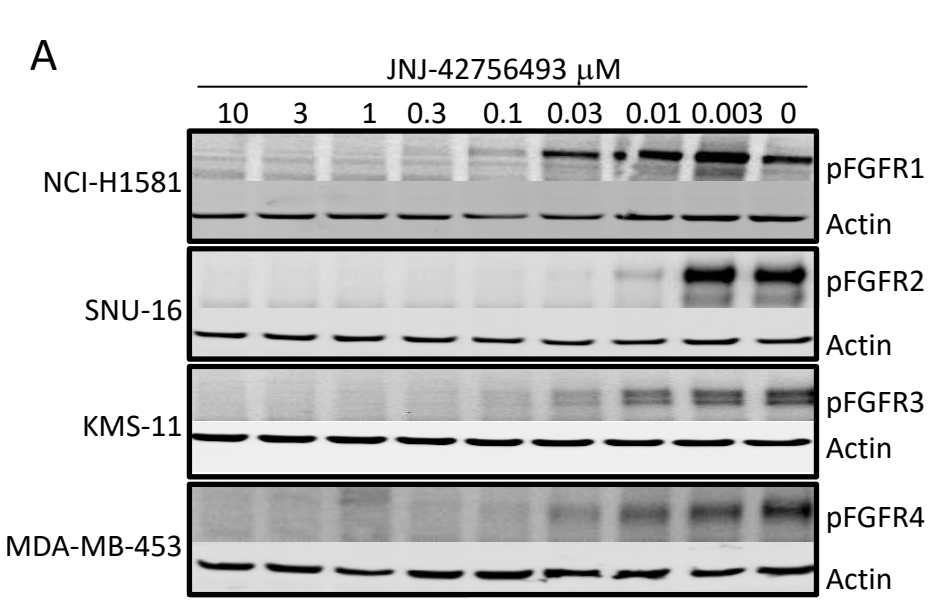

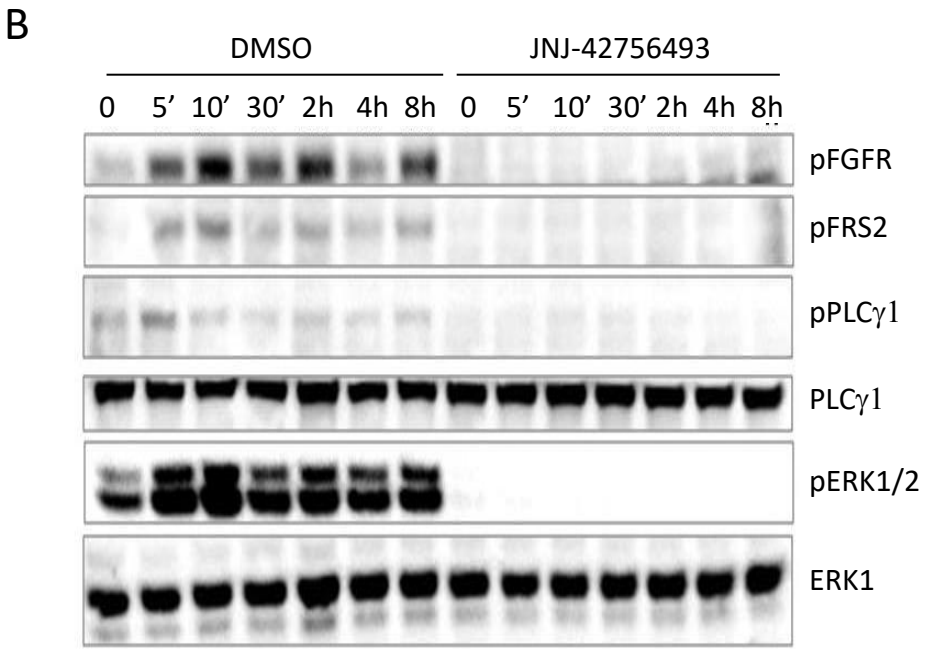

Figure 2

A

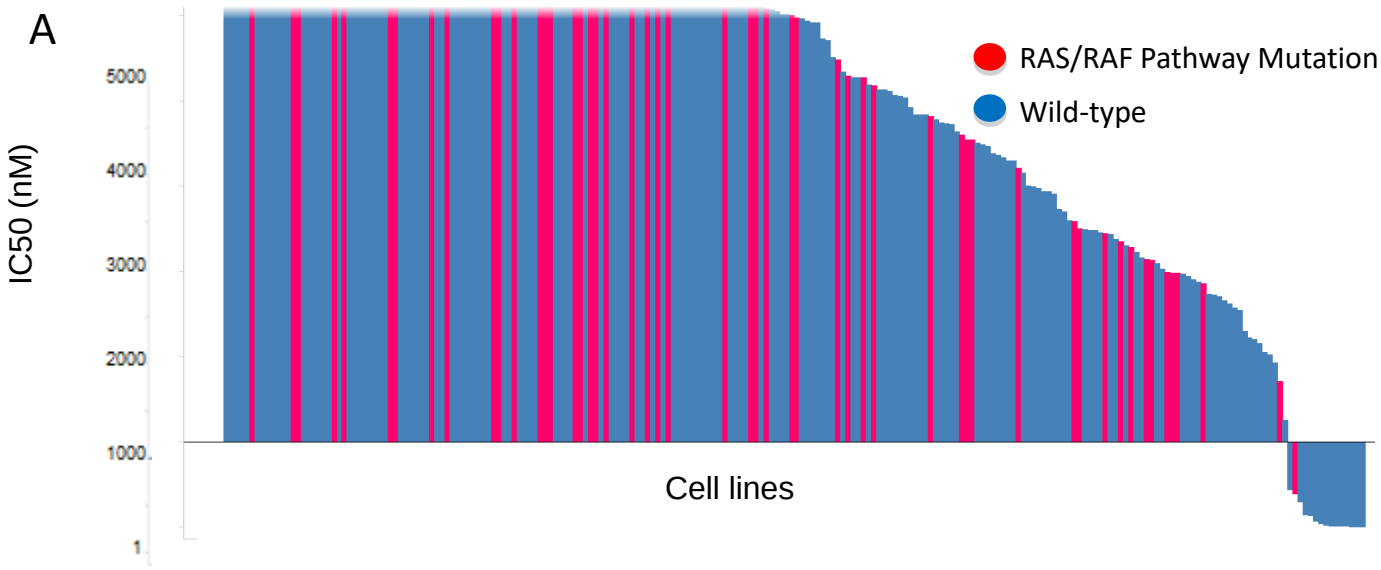

B

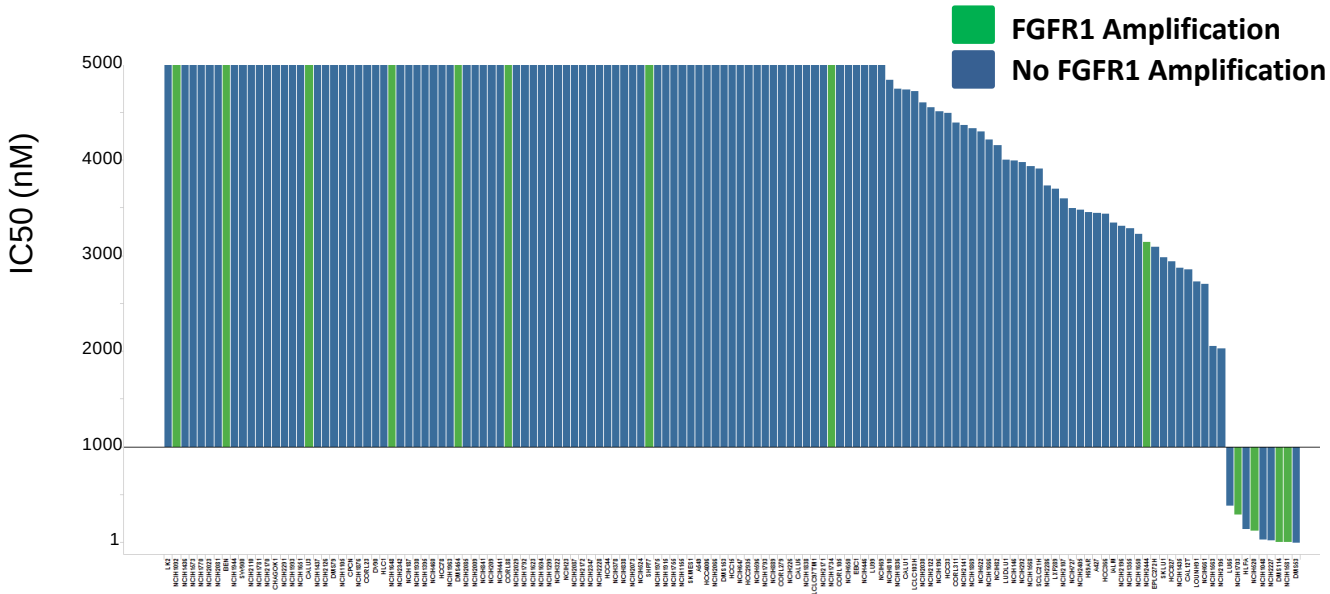

C

FGFR1 Amplified Cell Line	EGFR/KRAS Status
DMS114	WT
NCIH1581	WT
NCIH1703	WT
NCIH520	WT
BEN	EGFR Amplification
CALU3	EGFR Amplification
CORL88	KRAS Amplification
DMS454	WT
NCIH1092	WT (EGFR G482G)
NCIH1648	WT
NCIH1734	EGFR Amplification, KRAS G13C
NCIH2444	KRAS G12V
SHP77	EGFR Q701R, KRAS G12V

Figure 3

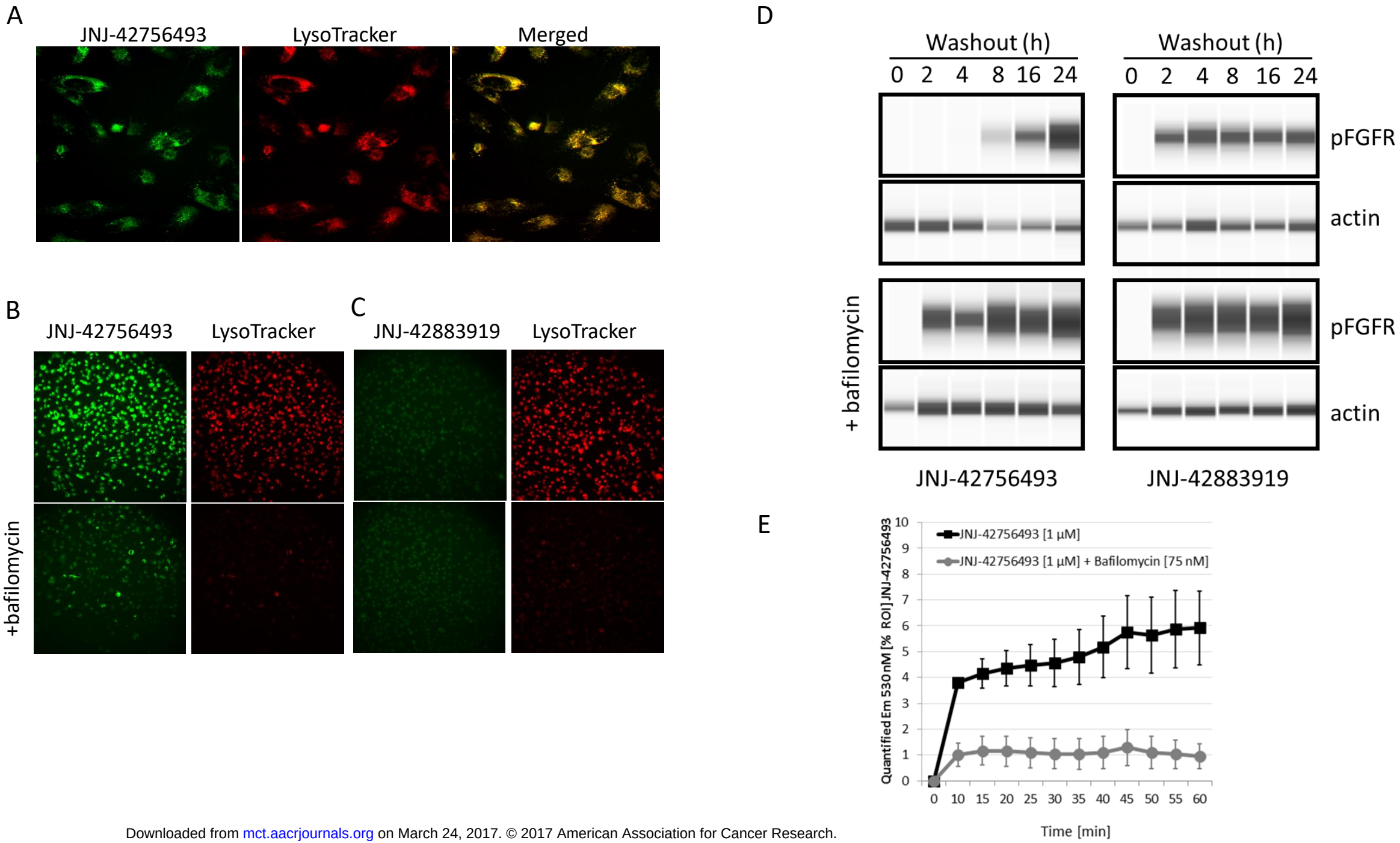

Figure 4

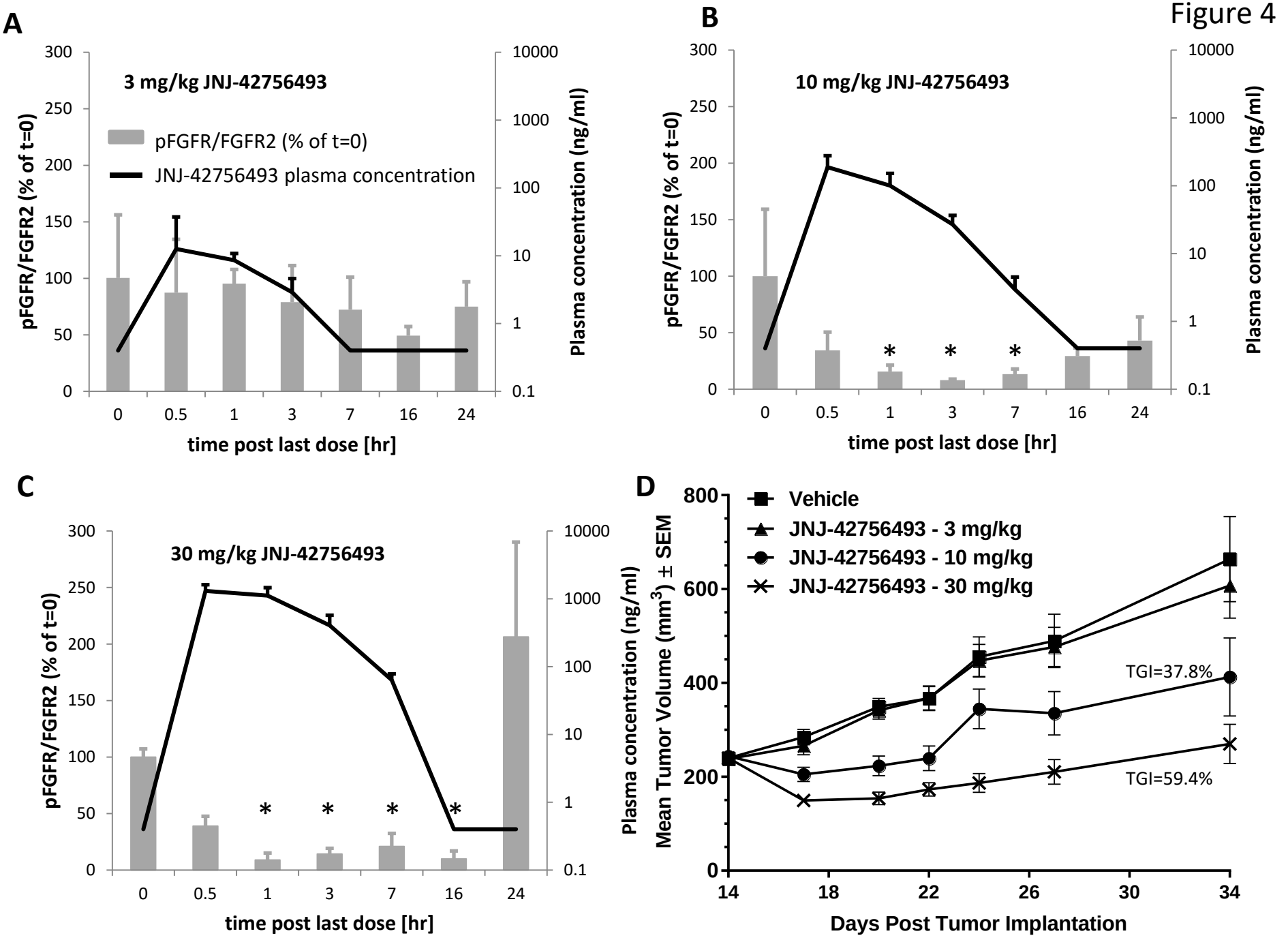

Figure 5

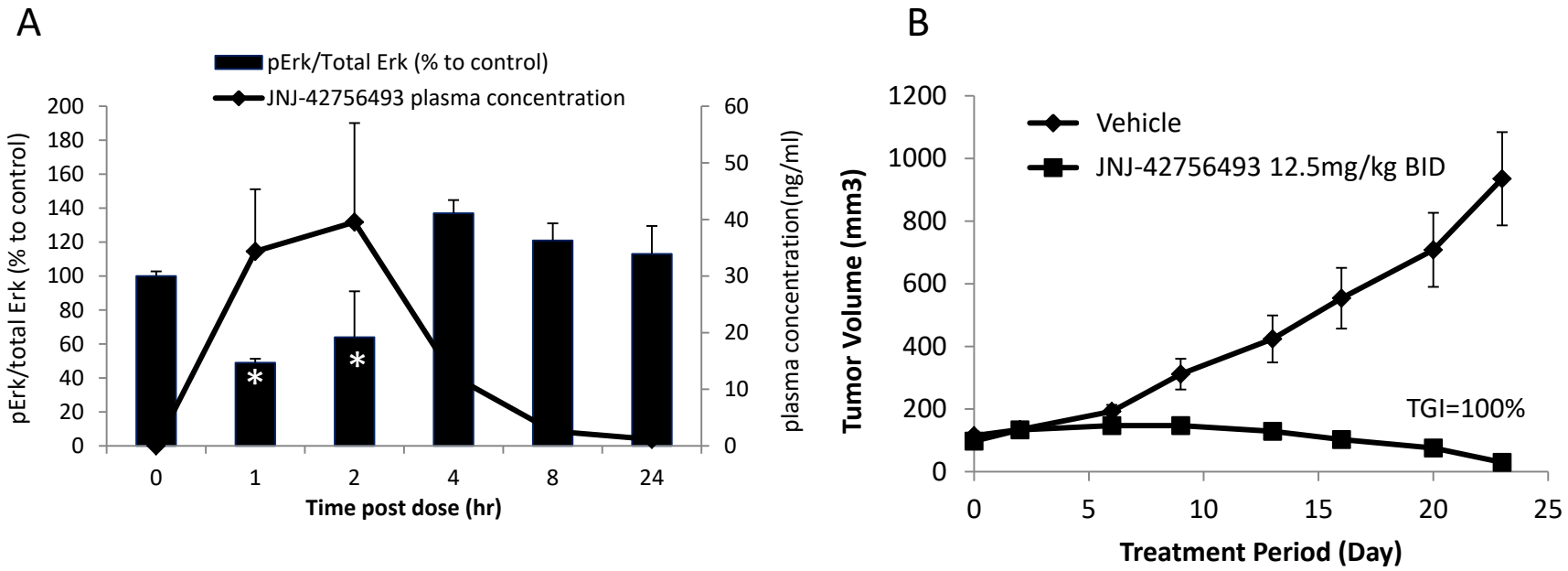

AACR American Association for Cancer Research

Molecular Cancer Therapeutics

Discovery and pharmacological characterization of JNJ-42756493 (erdafitinib), a functionally selective small molecule FGFR family inhibitor

Timothy P.S. Perera, Eleonora Jovcheva, Laurence Mevellec, et al.

Mol Cancer Ther Published OnlineFirst March 24, 2017.